DIFFRACTION IN OWL: EFFECTS OF SEGMENTATION AND SEGMENTS EDGE MISFIGURE

N. Yaitskova*[a], K. Dohlen[b], P. Dierickx[a]
[a]European Southern Observatory
[b]Laboratoire d'Astrophysique de Marseille

ABSTRACT

We consider the diffraction by segmented apertures with a very large number of segments, concentrating mostly on the effects which lead to the appearance of regular patterns of diffraction peaks, specific to extremely large telescopes (ELT). These effects are associated to gaps between segments, turned down/up segment edges and random tip-tilt errors. We discuss briefly the effect of segment piston error, which does not produce the higher-order diffraction peaks, but also affect the image quality. We deliver an analytical expression of the Point Spread Function (PSF) associated to each particular case and approximate formulae for the Strehl ratio and relative intensity of higher-order diffraction peaks.

Keywords: segmented mirrors, ELT, OWL, diffraction, PSF.

1. INTRODUCTION

Diffraction effects caused by an aperture with a large number of segments (hereafter strongly segmented aperture) differ qualitatively from those associated to apertures with a few segments. A segmented surface acts as a giant bi-dimensional diffraction grating, producing an interference pattern with regular peaks.[1-4] Although the intensity of higher-order diffraction peaks is 10^{-4} – 10^{-5} times the intensity of the central peak, in a giant telescope higher order effects must be accounted for. This is particularly important when looking for extra solar planets, which have a ratio of brightness to their parent star of ~10^{-9}. Moreover, while for a 1.5m flat-to-flat hexagonal segment and a wavelength of 0.5μm the first peak occurs at 0.08″ from the central peak, Earth-like planets are expected at 0.1″ - 0.2″ from their parent star.[5] Therefore, knowledge of the position and relative intensity of the diffraction peaks is essential.

The first part of the present paper is a general description of the PSF for a segmented telescope. Next, we consider the effect of gaps, turned up/down edges, and tip-tilt errors, emphasizing the diffraction effects. We discuss the piston error effect only briefly, because it does not lead to the appearance of a regular diffraction pattern and therefore is not particular for the ELT.

Our final goal is to find the Strehl ratio and the relative intensity of higher-order diffraction peaks at different angular distances. The results of all considered effects are presented in a table useful for practical applications.

2. PSF FOR SEGMENTED TELESCOPE

We consider (Figure 1) a segmented primary mirror consisting of N segments with a segmentation geometry similar to that of the Keck, i.e., organized in M concentric hexagonal “rings” around the central segment. The total number of segments (including the central one) is given by N = 3M(M+1)+1.

The expression of the PSF for a segmented mirror is presented in several recent publications.[1-4] In general it takes the form:

$$\mathrm{PSF}(\mathbf{w}) = \left(\frac{AN}{\lambda z}\right)^2 \left| \frac{1}{N} \sum_{j=1}^{N} \left[\exp\left(i \frac{2\pi}{\lambda z} \mathbf{w} \cdot \mathbf{r}_j \right) \frac{A_j}{A} \frac{1}{A_j} \int \theta_j(\xi) \exp\left[i\varphi_j(\xi) \right] \exp\left(i \frac{2\pi}{\lambda z} \mathbf{w} \cdot \xi \right) d^2\xi \right] \right|^2 . \quad (1)$$

Here **w** is the position vector in the image plane, z is the focal distance, λ is the wavelength; $\mathbf{r}_j$, A_j, θ_j, and φ_j are the position vector, the real area, transmission and phase functions of the j^{th} segment, respectively. We introduce the ideal area of the segment A, which for hexagonal segments is $\sqrt{3}d^2/2$. A flat-to-flat width d of an ideal segment coincides with the center-to-center distance between contiguous segments in Y-direction.

In the case of a perfectly phased telescope without intersegment gaps and with optically perfect segments (φ_j=0, A_j=A and θ_j=θ, for all segments), Eq. 1 takes the form:

$$\mathrm{PSF}(\mathbf{w}) = \left(\frac{\mathrm{AN}}{\lambda z}\right)^2 \left|\frac{1}{\mathrm{N}}\sum_{j=1}^{\mathrm{N}} \exp\left(\mathrm{i}\frac{2\pi}{\lambda z}\mathbf{w}\cdot\mathbf{r}_j\right)\right|^2 \left|\frac{1}{\mathrm{A}}\int \theta(\xi)\exp\left[\mathrm{i}\frac{2\pi}{\lambda z}\mathbf{w}\cdot\xi\right]\mathrm{d}^2\xi\right|^2 = \left(\frac{\mathrm{AN}}{\lambda z}\right)^2 \mathrm{GF}(\mathbf{w})\,\mathrm{PSF}_s(\mathbf{w}). \tag{2}$$

As in the case of a diffraction grating, the PSF of a segmented mirror can be represented as the product of two factors, regardless of the segmentation geometry: a "grid factor" (GF) which is the Fourier transform of the segmentation grid, usually a periodic function of sharp peaks, and the point spread function of an individual segment (PSF_s).

With a hexagonal geometry the analytical expression for GF is[1,3]:

$$\begin{aligned}\mathrm{GF}(\mathbf{w}) = \Bigg\{ &\sin\left[(3\mathrm{M}+1)\beta + (\mathrm{M}+1)\sqrt{3}\alpha\right]\frac{\sin\left[\mathrm{M}\left(\beta-\sqrt{3}\alpha\right)\right]}{\mathrm{N}\sin(2\beta)\sin\left(\beta-\sqrt{3}\alpha\right)} \\ &+ \sin\left[(3\mathrm{M}+2)\beta - \mathrm{M}\sqrt{3}\alpha\right]\frac{\sin\left[(\mathrm{M}+1)\left(\beta+\sqrt{3}\alpha\right)\right]}{\mathrm{N}\sin(2\beta)\sin\left(\beta+\sqrt{3}\alpha\right)}\Bigg\}^2,\end{aligned} \tag{3}$$

where

$$\alpha = (\pi d/2\lambda z)\mathrm{w}_x \text{ and } \beta = (\pi d/2\lambda z)\mathrm{w}_y \tag{4}$$

are normalized coordinates in the image plane. The grid factor corresponds to a hexagonal grid of sharp peaks whose location is defined by the conditions:

$$\begin{cases} 2\beta = \mathrm{m}\pi \\ \beta \pm \sqrt{3}\alpha = \mathrm{n}\pi \end{cases} \quad \text{or} \quad \begin{cases} \mathrm{w}_y = \mathrm{m}\lambda z/d \\ \mathrm{w}_y \pm \sqrt{3}\mathrm{w}_x = \mathrm{n}\,2\lambda z/d \end{cases}, \tag{5}$$

where *n* and *m* are integer values. For the following analysis it is important to point out that the value of all peaks in the GF equals to unity regardless of M. The geometry of the GF is shown in Figure 2. (To convert the coordinates in the image plane into units of radians we must omit a focal distance in Eqs. 5, i.e. substitute λz/*d* by λ/*d*.)

Because of the shape of the hexagonal grid, the Fourier image has a π/3 symmetry. This means that the PSF does not change if rotated by steps of π/3. For example, diffraction along any direction shown as a solid line in Figure 2 is the same as along axis α (in the following referred to as the A family). Along these directions, higher-order peaks are located equidistantly with radial steps of $\pi/\sqrt{3}$. The same is valid for any of the direction shown as a dashed line in Figure 2 (referred to as the B family). These peaks have a regular separation of π.

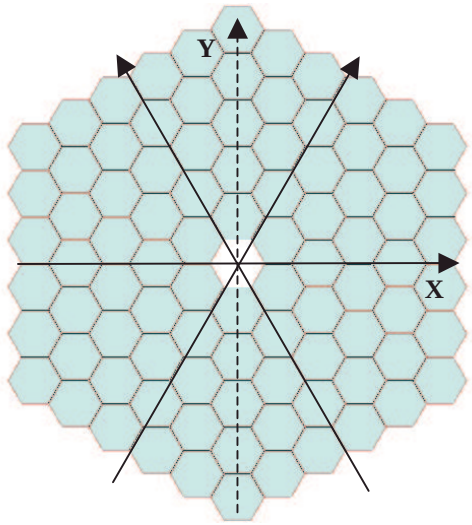

Figure 1. Segmented mirror. Segment number N=90, segmentation order M=5. Solid arrows illustrate the $\pi/3$ symmetry.

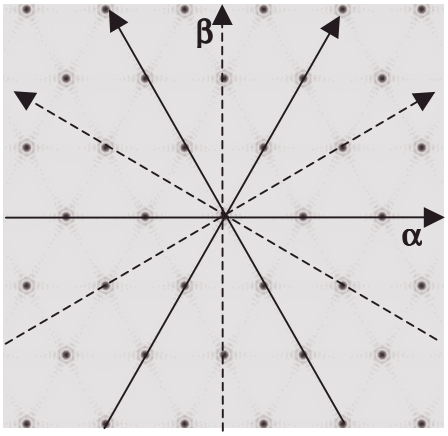

Figure 2. Grid factor. The $\pi/3$ symmetry is maintained in the Fourier plane: peaks are located equidistantly along any solid (dashed) line.

The segment PSF_s is the square modulus of the segment amplitude function, $t(\mathbf{w})$, which for hexagonal segments is

$$\begin{aligned} t(\mathbf{w}) &= \frac{1}{A}\int \theta(\xi)\exp\left(i\frac{2\pi}{\lambda z}\mathbf{w}\cdot\xi\right)d^2\xi \\ &= \frac{\sin\left(\sqrt{3}\alpha-\beta\right)\mathrm{sinc}\left(\alpha/\sqrt{3}+\beta\right)+\sin\left(\sqrt{3}\alpha+\beta\right)\mathrm{sinc}\left(\alpha/\sqrt{3}-\beta\right)}{2\sqrt{3}\alpha}, \end{aligned} \tag{6}$$

with α and β given by Eq. 4. The Eq. 6 is important for all following analysis since it allows to derive the exact analytical expression for the Strehl ratio and relative intensity of higher-order diffraction peaks associated with gaps, segment edge misfigure and tip-tilt error.

3. ANALYSIS OF DIFFRACTION EFFECTS

3.1. Gaps

Gaps are introduced by a shrinking the segment size from its ideal size given by the plane geometry of the hexagonally packed array. Consider the case when the segment is a perfect hexagon with its center at the ideal position, but where flat-to-flat width, d', is slightly smaller than the center-to-center distance, d. For analytical convenience we introduce ω, the relative gap size:

$$\omega = \frac{d - d'}{d} = 1 - d'/d\,. \tag{7}$$

If we assume segments to be identical in size and shape, then the area of the segment A' and the transmission function $\theta'(\xi)$ in Eq. 1 are independent of the index j. That allows to express the PSF as a product of the GF and the segment PSF_s:

$$PSF(\mathbf{w}) = \left(\frac{AN}{\lambda z}\right)^2 GF(\mathbf{w})PSF_S'(\mathbf{w},\omega)\cdot \tag{8}$$

While the GF is still defined by Eq.3, the segment PSF_s has become:

$$PSF_S'(\mathbf{w}) = \left| (1-\omega)^2 \frac{1}{A'} \int \theta'(\xi) \exp\left[i \frac{2\pi}{\lambda z} \mathbf{w} \cdot \xi \right] d^2\xi \right|^2 . \quad (9)$$

This function is defined only by the shape of an individual segment. As we will see, this approach is convenient to describe different diffraction effects associated with the strongly segmented mirrors.

As the GF is equal to unity at the center of the image coordinate system and in all points whose coordinates obey Eq. 5, for the calculation of the Strehl ratio and the intensity of higher-order diffraction peaks we need only to calculate the value of function $PSF_S'(\mathbf{w})$ in these coordinates.

From Eq. 9 we obtain the expression for the Strehl ratio, defined as the ratio of central peak intensity with gaps to the same intensity without gaps:

$$S = (1-\omega)^4 \approx 1 - 4\omega + 6\omega^2 , \quad (10)$$

i.e. the loss of the Strehl ratio is – unsurprisingly – equal to the square of the ratio (gap total area/ aperture area).

Assuming 1.5 m segments with gaps of 12 mm (plausible value for OWL), the relative gap size is $\omega = 0.008$, and the Stehl ratio equals to 0.98. This relatively small energy loss is accompanied, however, by the appearance of a diffraction pattern, which could possibly complicate the scientific exploitation of data.

The location of the GF peaks is defined by the distance between segment centers and does not change with gap size. With an increase of gap size (decrease of segment size), the PSF_S' widens, its zeroes move outwards, and the GF peaks are revealed (Figure 3b). In the following, all peaks except for the central one are referred to as higher-order peaks.

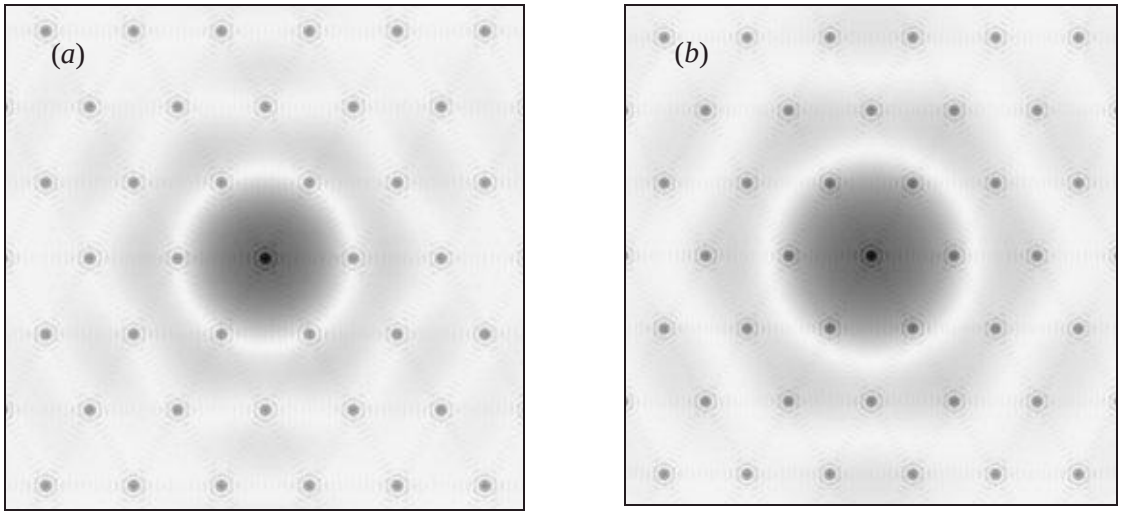

Figure 3. Grid factor and segment PSF for a perfect mirror without gaps (a), and for a mirror with gaps between segments (b).

We are now interested in the ratio of higher-order peak to the central peak intensity. From now on, we refer to this ratio as the higher-order peak relative intensity.

Due to the symmetry, peaks located at a fixed angular distance from the center have equal intensity. Figure 4 shows all peaks out to 0.32" according to their angular distance from the center (segment size 1.5m flat-to-flat). They are labeled with a family name and an order number. Each family of peaks can be defined by its initial angle from horizontal:

Family A: $n(\pi/3)$;
Family B: $\pi/6+n(\pi/3)$;
Family C: $\arctan(\sqrt{3}/5)+n(\pi/3)$ and $\arctan(\sqrt{3}/2)+n(\pi/3)$;
Family D: $\arctan(\sqrt{3}/7)+n(\pi/3)$ and $\arctan(3\sqrt{3}/2)+n(\pi/3)$.

The number of possible families is infinite; in the following we concentrate only on those represented within a 0.32" radius.

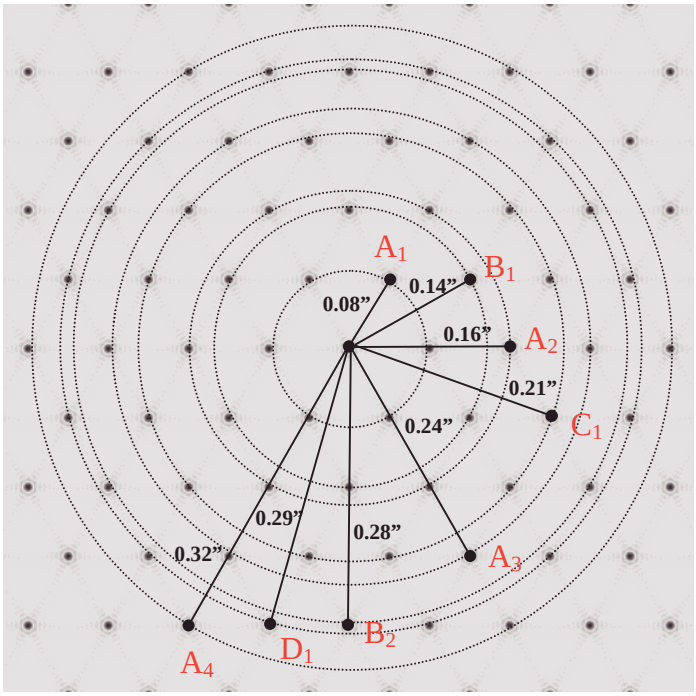

Figure 4. Symmetry in the diffraction pattern: all peaks belonging to the same circle have equal intensity. Segment size d=1.5m, λ=0.5μm.

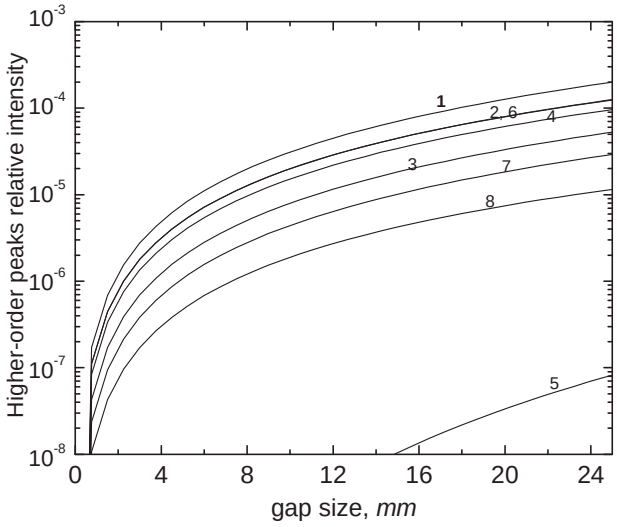

Figure 5. Relative intensity of higher-order peaks as a function of gap size, λ = 0.5 μm, d=1.5m. The curve index corresponds to the group of peaks at angles:

1: 0.08″ (A_1)
2: 0.14″ (B_1)
3: 0.16″ (A_2)
4: 0.21″ (C_1)
5: 0.24″ (A_3)
6: 0.28″ (B_2)
7: 0.29″ (D_1)
8: 0.32″ (A_4)

The higher-order peak relative intensity is plotted as a function of gap size in Figure 5. Although all the curves are monotonous within the plotted range, peaks at larger angles are not always weaker than peaks located closer to the center. For example, the series of peaks to be found at 0.16″ (A_2) are fainter than peaks located at 0.21″ (C_1). A more thorough discussion of these phenomena will be given in a future paper. However, it is important to note that the structure of higher-order peaks in a hexagonal segmentation geometry is very different from that of a square segmentation geometry. In the latter case, a single family of peaks is observed, repeated along two orthogonal directions. In close analogy with the simple 1D case (classical diffraction grating), the peaks are of similar amplitude out to an angular separation of about $\lambda/(d\omega)$. In the hexagonal case, such a behavior is observed for the B family peaks as can be seen in Figure 5 where curves 2 (B_1) and 6 (B_2) are coincident.

The brightest peaks are the six A_1 peaks at 0.08" from the center. The relative intensity of these peaks for small ω is

$$I_{A1}(\omega) \approx 0.7\omega^2 . \tag{11}$$

Taking as an average for OWL 12mm gap and 1.5m segments, we obtain: $I_{A1}(w=0.008)= 4\cdot10^{-5}$.

It should be noted, however, that this figure is quite conservative. With all identical segments, OWL has gap size varying from ~6mm to ~18mm, and the projected geometry of the primary mirror is slightly irregular. As a result the higher-order peaks will be blurred, in addition to the effect of pupil rotation.

3.2. Turned Down/Up Edge

We refer to turned down/up edges to describe residual polishing errors in the form of phase profile misfigure appearing on the edge of the segments (Fig. 6). We introduce two important parameters: width of misfigure η, and depth ε. To model this effect, different functions for the edge profile can be used. On the basis of practical experience we assume a quadratic function:

$$\varphi(x, \varepsilon, \eta) = -\varepsilon\left(x/\eta\right)^2 . \tag{12}$$

Point x=0 corresponds to the "beginning" of the misfigure, x=η to the edge of the segment.

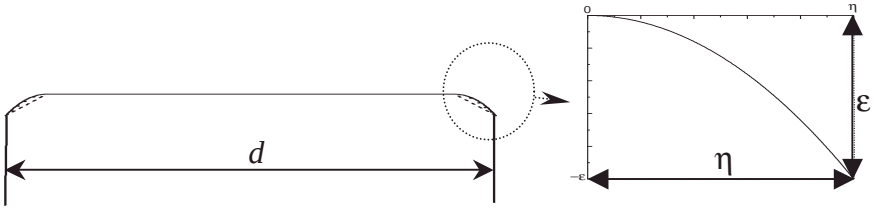

Figure 6. Turned down edge with a quadratic phase profile on the segment edge.

We assume equivalent edge shape for all segments; the PSF can be presented as the product of the grid factor GF, introduced in Eq. 3, and the modified segment PSF, PSF_s':

$$PSF(\mathbf{w}) = \left(\frac{AN}{\lambda z}\right)^2 GF(\mathbf{w}) PSF_S'(\mathbf{w}, \eta, \varepsilon) \cdot \tag{13}$$

By analogy with effects of gaps, to calculate the Strehl factor and the intensity of higher-order maxima, we have to derive an expression for the PSF_s'. The detailed calculation technique will be presented in a future paper. Here we present the final expression for the PSF_s':

$$PSF_S'(\mathbf{w}, \eta, \varepsilon) = \left| \left(\frac{d-2\eta}{d}\right)^2 t(\mathbf{w}, 0, \eta) + \int_0^{\eta} \exp[i\varphi(x, \eta, \varepsilon)] \frac{\partial}{\partial x}\left[\left(\frac{d-2\eta+2x}{d}\right)^2 t(\mathbf{w}, x, \eta)\right] dx \right|^2 \cdot \tag{14}$$

In this expression $\partial[F(x)]/\partial x$ is the partial derivative of F(x) over x and $\varphi(x, \eta, \varepsilon)$ is the phase profile at the segment edge (Eq. 12). The segment amplitude function $t(\mathbf{w}, x, \eta)$ is given by Eq. 6 with

$$\alpha = [\pi(d - 2\eta + 2x)/2\lambda z] w_x \quad \text{and} \quad \beta = [\pi(d - 2\eta + 2x)/2\lambda z] w_y. \tag{15}$$

The amplitude function $t(\mathbf{w}, x, \eta)$ is equal to unity at point $\mathbf{w}$=0 for all x. For the Strehl ratio we obtain:

$$S(\eta, \varepsilon) = \left| \left(\frac{d-2\eta}{d}\right)^2 + \int_0^{\eta} \exp[i\varphi(x, \eta, \varepsilon)] 4 \frac{d-2\eta+2x}{d^2} dx \right|^2 \cdot \tag{16}$$

The exact analytical expression for the Strehl ratio can be evaluated assuming the quadratic phase function. The curves as a function of ε are shown in Fig. 7 for η=5, 10 and 20mm, d=1.5m. Note that the curves saturate to $(1- 2\eta/d)^4$. The saturation level of the Strehl ratio does not depend on the segment edge shape. In this limit, the integrand of the second term in Eq. 16 is a fast oscillating function, the integral of which for finite limits tends to zero. For any $\varphi(x, \eta, \varepsilon)$ the saturation level is equal to the ratio $[(d-2\eta)/d]^4$. That is not surprising: infinitely deep slopes play the same role as amplitude gaps with a relative size ω=2η/d, and the Strehl ratio in that limit is described by Eq. 10. For any given η, the Strehl ratio does not decrease beyond its saturation level and we could use this level as a lower limit of $S(\eta, \varepsilon)$. However, this is arguably over-conservative. In practice the depth ε is not expected to exceed ~2π radians. The minimum of $S(\eta, \varepsilon)$ in this range gives us a convenient estimate for the Strehl ratio, especially because the position of the minimum does not depend on η:

$$S(\eta, \varepsilon) > 1 - 3.3\left(\frac{2\eta}{d}\right) + 4.5\left(\frac{2\eta}{d}\right)^2. \tag{17}$$

This gives 0.98, 0.95 and 0.92 for η=5, 10 and 20mm correspondingly.

In the case of OWL, surface edge misfigure is expected to be in the range of a quarter wave length and to extend over 20 -10mm of a segment area (we assume the stress – free polishing on planetary polishers). This leads to an expected Strehl ratio in a range 0.94 - 0.97.

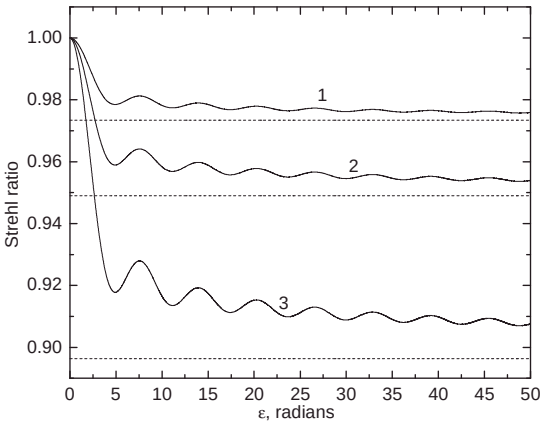

Figure 7. Strehl ratio for turned down edges as a function of misfigure depth. The curve parameter is misfigure width. 1: η=5mm; 2: η=10mm; 3: η=20mm. Segment size *d*=1.5m. Dashed lines are the saturation level $(1- 2\eta/d)^4$.

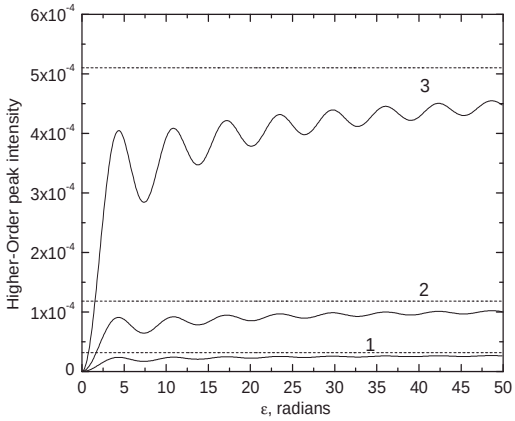

Figure 8. Relative intensity of higher-order peaks A_1. 1: η=5mm; 2: η=10mm; 3: η=20mm. Segment size *d*=1.5m. Dashed lines are saturation level $0.7\cdot(2\eta/d)^2$.

The intensity of the higher-order peaks is given by the PSF'$_S$ of Eq. 14, where $t(\mathbf{w}, x, \eta)$ is calculated using points with coordinates from Eq. 5. We present here only the final expression for the brightest A_1 peaks. In Fig.6 there are six peaks located at 0.08" from the center:

$$I_{A1}(\eta, \varepsilon) \approx \left(\frac{2\eta}{d}\right)^2 \mathrm{sinc}^2\left(\frac{\pi}{3}\right)\left\{1-\sqrt{\frac{\pi}{2\varepsilon}}\,C\left(\sqrt{\varepsilon}\right)+\frac{\pi}{2\varepsilon}\left[C^2\left(\sqrt{\varepsilon}\right)+S^2\left(\sqrt{\varepsilon}\right)\right]\right\}, \tag{18}$$

where $C\left(\sqrt{\varepsilon}\right)$ and $S\left(\sqrt{\varepsilon}\right)$ are the Fresnel integrals:

$$C(x)=\sqrt{\frac{2}{\pi}}\int_0^x \cos\left(t^2\right)dt; \quad S(x)=\sqrt{\frac{2}{\pi}}\int_0^x \sin\left(t^2\right)dt. \tag{19}$$

Eq. 18 is valid for any parameter ε. Again, this is an approximation to $(\eta/d)^2$ accuracy. The curves for η=5, 10 and 20mm and *d*=1.5m are shown in Fig. 8. As we did above for the Strehl ratio we estimate the upper level of I_{A1} within a range ε=0…2π by the value of its maximum, whose position in this case is independent of η. So the intensity of these peaks is no higher than

$$I_{A1}(\eta, \varepsilon) < 0.5\left(\frac{2\eta}{d}\right)^2. \tag{20}$$

For η=5, 10 and 20mm the estimation is $2\cdot10^{-5}$, $8.5\cdot10^{-5}$ and $4\cdot10^{-4}$ correspondingly.

These estimates shall be deemed as very pessimistic, as the expected surface misfigure for OWL segment edges should be of ¼ wavelength. Then the expected values for I_{A1} peaks relative intensity is $7\cdot10^{-5}$ - $3\cdot10^{-4}$.

3.3. Tip-Tilt Effect

A detailed analysis of diffraction effects associated with tip-tilt errors for mirrors with a large number of segments can be found elsewhere.[1] Here we present the main results of the study because in many respects they are similar to that caused by gaps or turned up/down edges.

An aperture with random segments tip-tilt errors behaves as a randomly blazed diffraction grating. The loss of intensity in the central peak is accompanied by the appearance of regular diffraction peaks around the central one on a background of random speckles. The PSF consists of two terms: the first item describes the regular diffraction pattern; the second item describes the non-regular speckle field. The former is nearly independent of segment number, although the intensity of the non-regular component decreases as N^{-1}. For a small number of segments the regular pattern "is lost" in speckles, but for large N it dominates.

As the main object of the present paper is the diffraction effects associated to strong segmentation, we assume that the non-regular component is negligible and in the following we concentrate on the regular term. As in Eqs. 8 and 13 the ensemble averaged PSF (its regular part) is a multiplication of the grid function GF and a modified PSF for one segment:

$$\left\langle \mathrm{PSF}(\mathbf{w},\mathrm{rms})\right\rangle \approx \left(\frac{\mathrm{AN}}{\lambda z}\right)^2 \mathrm{GF}(\mathbf{w})\,\mathrm{PSF}_S'(\mathbf{w},\mathrm{rms})\cdot \tag{21}$$

The GF is again the grid factor from Eq. 3. The modified $\mathrm{PSF}_S'(\mathbf{w},\mathrm{rms})$ depends on the tip-tilt rms. So we observe the analogy with the modified segment PSF from Eqs. 9 and 14. The following analysis is directly analogous with those presented in subsections 3.1 and 3.2.

The modified $\mathrm{PSF}_S'(\mathbf{w},\mathrm{rms})$ was found to be[1]

$$\mathrm{PSF}_s'(\mathbf{w},\mathrm{rms}) = \left|\int\ \mathrm{t}(\mathbf{w}')\mathrm{Q}(\mathrm{rms},\mathbf{w}-\mathbf{w}')\mathrm{d}^2\mathrm{w}'\right|^2, \tag{22}$$

where the function t(**w**) is the segment amplitude function (6), and $\mathrm{Q}(\mathrm{rms},\mathbf{w}-\mathbf{w}')$ is a Gaussian function with a width equal to 2.7rms:

$$\mathrm{Q}(\mathrm{rms},\mathbf{w}-\mathbf{w}') = \left(\frac{2\pi}{\lambda z}\right)^2 \frac{d^2}{2\pi(2.7\,\mathrm{rms})^2}\exp\left[-\left(\frac{2\pi}{\lambda z}\right)^2 \frac{(\mathbf{w}-\mathbf{w}')^2 d^2}{2(2.7\,\mathrm{rms})^2}\right]. \tag{23}$$

The ensemble averaged Strehl ratio is the value of $\mathrm{PSF}_S'(\mathbf{w},\mathrm{rms})$ for the point **w**=0. The curves are presented in Fig. 9 for N=37, 217, and 817. For a small tip-tilt rms value the Strehl ratio can be approximated as the following:

$$\mathrm{S}(\mathrm{rms}) \approx 1-\mathrm{rms}^2+\frac{\mathrm{rms}^4}{4}\left(2.34+\frac{2}{\mathrm{N}}\right)\cdot \tag{24}$$

To the second order, this expression coincides with the Marechal approximation. Note the weak dependence on number of segments which is in contrast to the case of pure piston errors[2,6] where the Strehl ratio reaches a floor level equal to 1/N.

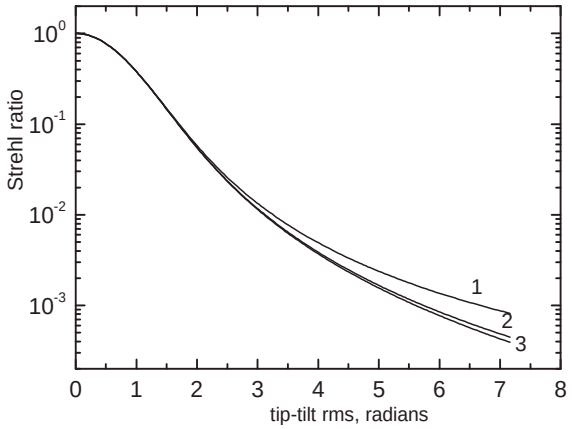

Fig. 9. Strehl ratio as a function of tip-tilt rms for different numbers of segments:
1: N=37; 2: N=217; 3: N= 817.

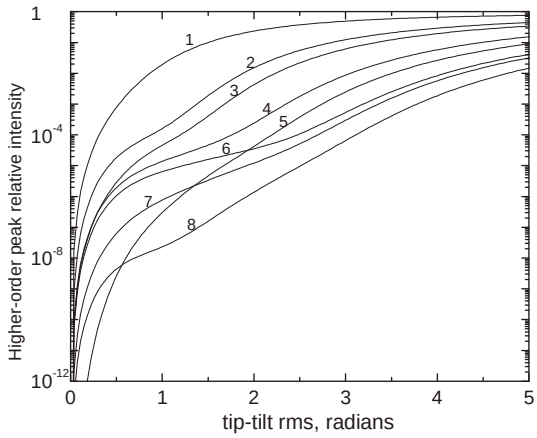

Fig. 10. Relative intensity of higher-order peaks as a function of tip-tilt rms. N=217. The curve index corresponds to the group of peaks at a definite angle: 1: 0.08″(A_1); 2: 0.14″(B_1); 3: 0.16″(A_2); 4: 0.21″(C_1); 5: 0.24″(A_3); 6: 0.28″(B_2); 7: 0.29″(D_1); 8: 0.32″(A_4).

The position of higher-order peaks is defined by the GF and their value can be calculated from the $\mathrm{PSF}_S'(\mathbf{w}, \mathrm{rms})$ using points from Eq. 5. Unlike the effects considered above, the intensity of peaks with the same index and order are not equal anymore. For example, there is a slight difference in the intensities of the six A_1 peaks for a short exposure image. We can create analytical expressions only for ensemble averaged characteristics. A more precise statistical analysis can be found elsewhere.[1]

The ensemble averaged relative intensity of higher-order diffraction peaks is shown in Fig. 10 for N=217. Like the Strehl ratio, the intensity of the peaks for large N is insensitive to the number of segments. The curve saturation is the result of normalization: for large rms the higher-order peaks decrease according to the same law as the Strehl ratio.

As we did above, we present here the approximate expression for the averaged intensity of A_1 peaks for the small rms:

$$I_{A1}(\mathrm{rms}) \approx 0.013\mathrm{rms}^4 . \tag{25}$$

Taking as a reasonable estimate for OWL a tip-tilt rms=λ/30, we obtain S=0.96 and $I_{A1}=2.5\cdot10^{-5}$.

3.4. Piston Effect

Although the main intention of the present paper is to enclose all effects which lead to the appearances of the diffraction pattern, the piston effect should not be set aside.

The PSF for the segmented aperture with random piston distribution can be represented as a product of the GF and segmented PSF. But unlike in all previous cases, the presence of piston errors does not change the segment PSF_s, but disturbs the periodic structure of the function GF. As the result in a whole PSF the noisy undergrowth of speckles appears, but not the diffraction pattern of the regular peaks.

The appearance of speckle is accompanied by a reduction in the Strehl ratio. The expression for the ensemble averaged Strehl ratio is[2,6]

$$S = \frac{1}{N}\left[1 + (N-1)\exp\left(-\mathrm{rms}^2\right)\right], \tag{26}$$

Note the saturation of the Strehl ratio to the level N^{-1}.

The angular size of speckle field does not depend on the piston rms and can be defined as a full width at half maximum of the PSF_s :

$$\varepsilon_{speckle} \approx 2.9\lambda/\pi d\,. \tag{27}$$

For λ=0.5μm and d=1.5m $\varepsilon_{speckle}$ ~0.07″.

The ratio R (averaged speckle/central peak intensity) can be found by applying energy conservation and the assumption that the average width of an each individual speckle is the same as the width of the central peak. If we use the fact that the number of speckles is equal to the number of segment N then we obtain:

$$R = \frac{1-\exp(-\mathrm{rms}^2)}{1+(1-N)\exp(-\mathrm{rms}^2)}\,. \tag{28}$$

The OWL expected piston rms is λ/30, that gives 0.96 for the Strehl ratio and $R = 3\cdot10^{-5}$ for the relative intensity of the speckled field.

4. RESULTS

We have presented a unified approach to the study of diffraction effects from gaps, segment edge misfigure, and random piston and tip-tilt errors. All considered effects lead to a loss of intensity in the central point and a disturbance of the PSF structure. Gaps and segment edge misfigure produce the regular pattern of the higher-order diffraction peaks, piston errors produce only the speckles, and tip-tilt errors – the combination of speckles and the higher-order peaks. For each effect, the telescope PSF can be represented as a product of the GF and the segment PSF_s, modified specifically for each case.

The Strehl ratio and the relative intensity of diffraction peaks can be found by calculating the segment PSF_s at the points where the peaks of the GF are located. For the Strehl ratio and the relative intensity of the six brightest peaks (A_1), approximate expressions have been obtained. We summarize the results in Table 1, in which numerical values for typical parameters are also shown.

Table 1. Strehl ratio and relative intensity of the first order diffraction peaks.

Effect	**Critical parameters**	**Typical value**	**Strehl ratio**		**Relative intensity of A_1 peaks**	
			Expression	**Value**	**Expression**	**Value**
Gap	gap size, δ segment size d	12mm 1.5m	$(1-\delta/d)^4$	0.98	$0.7(\delta/d)^2$	$4\cdot10^{-5}$
Turned edges	depth, ε width, η	0.25μm (WF) 20 -10mm	$> 1-3.3\cdot(2\eta/d)$ $+ 4.5\cdot(2\eta/d)^2$	0.94 - 0.97	$< 0.5(\eta/d)^2$	$7\cdot10^{-5}$ - $3\cdot10^{-4}$
Tip-tilt	rms segments, N	λ/30 (WF) 1600	$1-\mathrm{rms}^2$ $+ \mathrm{rms}^4(2.34+2/N)/4$	0.96	$0.013\mathrm{rms}^4$	$2.5\cdot10^{-5}$
Piston	rms segments, N	λ/30 (WF) 1600	$\exp(-\mathrm{rms}^2)$	0.96	—	—

5. CONCLUSION

The next generation of large telescopes will have highly segmented apertures. It is therefore important to study the optical effects caused by such segmentation. The four effects (gaps, segment edges misfigure, and random piston and tip-tilt errors) examined here are susceptible to analytical methods, creating the groundwork for accurate simulations.

Studying gaps, edges misfigure, and random tip-tilt errors we have concentrated on two main aspects: the Strehl ratio and the relative intensity of higher-order diffraction peaks. For the latter we suggest a classification, which distinguishes the peaks of different diffraction orders and takes into account the $\pi/3$ symmetry. The derived expressions provide a useful insight into the performance of highly segmented mirrors. Taking into account these effects will help designing the next generation of large telescopes.

REFERENCES

1. N. Yaitskova and K. Dohlen, "Tip-tilt error for extremely large segmented telescopes: detailed theoretical point-spread-function analysis and numerical simulation results," JOSA A/Vol. 19, No. 7, pp. 1274-1285 (2002).

2. N. Yaitskova and K. Dohlen, "Simulation of imaging performance for extremely large segmented telescopes," in *Optical Design, Materials, Fabrication, and Maintenance*, P. Dierickx, ed., Proc. SPIE **4003**, 279-290 (2000).

3. G. Zeider and E. Montgomery, "Diffraction effect with segmented aperture," in *Space Telescopes and Instruments V*, P. Bely, J. Breckinridge, eds., Proc. SPIE **3356**, 799-809 (1998).

4. G. Zeider, "Image-Based Alignment of Large Segmented Telescope," in *Optical Design, Materials, Fabrication, and Maintenance*, P. Dierickx, ed., Proc. SPIE **4003**, 241-249 (2000).

5. T.G. Hawarden, R. Gilmozzi, O. Hainaut, B. Leibundgut, G.F. Gilmore, M.R. Merrified, D. Queloz, R.F.G. Wyse and D. Dravins, "Critical science with the largest telescopes: science driver for a 100m ground-based optical - IR telescope," these proceedings #4840-55.

6. G. Chanan and M. Troy, "Strehl ratio and modulation transfer function for segmented mirror telescope as function of segment phase error," Appl. Opt. 38, pp. 6642-6647 (1998).

*nyaitsko@eso.org, phone +49 893200 6581; fax +49 89 320 2362, www.eso.org, ESO, Karl-Schwarzschild-Str. 2 D-85748 Garching bei München.